A hierarchically porous diatomite/silicalite-1 composite for benzene adsorption/desorption fabricated via a facile pre-modification *in situ* synthesis route

Weiwei Yuan [a,b], Peng Yuan [a,*], Dong Liu [a], Liangliang Deng [a,b], Junming Zhou [a,b], Wenbin Yu [c], Fanrong Chen [a]

[a] *CAS Key Laboratory of Mineralogy and Metallogeny/Guangdong Provincial Key Laboratory of Mineral Physics and Materials, Guangzhou Institute of Geochemistry, Chinese Academy of Sciences, Wushan, Guangzhou 510640, China*
[b] *University of Chinese Academy of Sciences, Beijing 100039, China*
[c] *State Key Laboratory of Ore Deposit Geochemistry, Institute of Geochemistry, Chinese Academy of Sciences, Guiyang, Guizhou 550002, China*

HIGHLIGHTS

- Diatomite/silicalite-1 composite was prepared by a mild pre-modification *in situ* coating route.
- This novel synthesized route increased the zeolite loading amount onto diatomite.
- The composite got macro-meso-microporous structure with high specific surface area.
- The composite exhibited excellent static and dynamic benzene adsorption behavior.
- The composite presented good reusability for benzene adsorption.

GRAPHICAL ABSTRACT
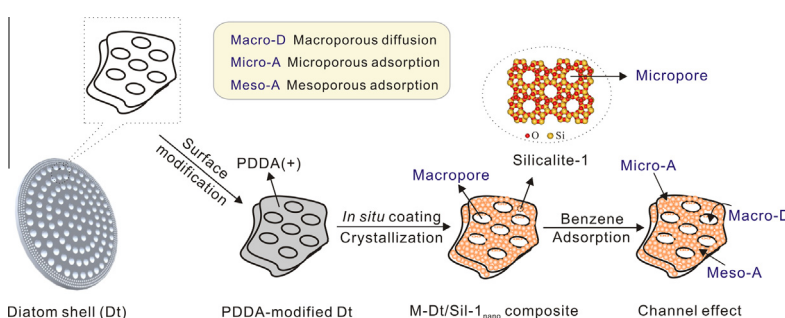
ARTICLE INFO

ABSTRACT

A novel, hierarchically porous diatomite/silicalite-1 composite with a high benzene removal efficiency was prepared via a facile coating process. Silicalite-1 nanoparticles (Sil-1$_{nano}$) were synthesized *in situ* on the surface of the pre-modified diatomite support by using a mild, low-temperature reflux reaction method. The obtained composite possessed a hierarchically porous structure, involving micropores and stacking mesopores from the silicalite-1 nanoparticles, and it retained the macropores from the diatomite support. The specific surface area and micropore volume of the composite were 348.7 m^2/g and 0.127 cm^3/g, respectively, with a zeolite loading amount of up to 60.2%. The diatomite/silicalite-1 composite exhibited considerably higher static and dynamic benzene adsorption capacities (94.9 mg/g (Sil-1$_{nano}$) and 246.0 mg/g (Sil-1$_{nano}$) respectively) per unit mass of zeolite than did the synthesized Sil-1$_{nano}$ and commercial ZSM-5. Moreover, the introduced macroporosity of the diatomite reduced the mass transfer resistance of the nanoparticles because of their improved dispersity, and it provided more possible entryways for benzene molecules, leading to better penetration of benzene than for Sil-1$_{nano}$ or commercial ZSM-5. The composite showed steady reversibility after 4 adsorption cycles, further demonstrating the promise of such a novel synthesized adsorbent for the removal of volatile organic compounds in industrial applications.

© 2016 Elsevier B.V. All rights reserved.

∗ Corresponding author. Tel./fax: +86 20 85290341.
  E-mail address: yuanpeng@gig.ac.cn (P. Yuan).

1. Introduction

In recent years, the emissions of volatile organic compounds (VOCs) from industrial processes have received considerable attention because of the severe environmental hazards they create. Most VOCs are toxic, carcinogenic, or even mutagenic and are the primary contributors to photochemical pollution and secondary organic aerosols [1–4]. Various technologies have been developed for VOC abatement, such as catalytic oxidation [5], adsorption [6], membrane separation [7] and biofiltration [8]. Of these available techniques, adsorption is widely accepted as the most effective VOC removal method because of its flexible operation (possible even at low concentrations), low costs and low energy consumption [6,9]. A key solution for the problems associated with this method is to seek out an alternative adsorbent with a high VOC removal efficiency.

Activated carbon has conventionally been used as a gas adsorbent because of its high porosity and low cost [10,11]. However, its poor thermal stability and limited modification flexibility prevent its industrial application in VOC adsorption. In addition, it is difficult to regenerate the active material because the organic gas molecules adsorbed in the slit-like micropores of activated carbon are difficult to desorb [12]. Silicalite-1, the most well-known aluminum-free MFI-type zeolite, exhibits a significant adsorption capacity for VOCs because of its abundance of microporous structures with high specific surface areas and well-developed hydrophobicity [13,14]; in particular, silicalite-1 nanoparticles, are characterized as having high thermal and chemical stabilities and favorable reusability. Compared with activated carbon, the orderly straight or zigzag channels (sinusoidal pore size of 0.54 nm and elliptical pores with a pore size of 0.51 nm × 0.57 nm) of the micropores are advantageous for the desorption of gas molecules [15].

However, two major issues still exist in the application of silicalite-1 nanoparticles as adsorbents: (i) nanoparticle agglomeration is widely known to lower the effective surface area and reduce reaction activity, leading to a low VOC adsorption capacity; and (ii) silicalite-1 nanoparticles exhibit monomodal microporosity with a pore size smaller than 1 nm. These structural micropores of silicalite-1 readily limit the diffusion and mass transfer of certain macromolecules such as m-xylene and o-xylene [16–18]. Coating the silicalite-1 nanoparticles onto macroporous supports for the fabrication of the hierarchically porous composite is an alternative strategy to overcome these problems. Nanoparticles dispersed on a macroporous support are capable of diminishing their agglomeration. In addition, the macroporous structure of the support shortens the diffusion path and reduces the resistance to gas penetration, increasing the mass transfer efficiencies of guest molecules. Various porous materials, including α-alumina [19,20], stainless steel [21], porous carbon discs [22] and ceramics [23], have been developed as supports for the preparation of hierarchically porous composites. Nonetheless, the pre-synthesis or pretreatment process of such supports may increase the synthesis costs of the composites. Moreover, the low porosities, poor thermal stabilities or inferior renewable performance constrain their application in industrial processes. Consequently, identifying desirable porous supports that are economically viable and have high porosities and recyclability is important for improving the VOC adsorption performance of silicalite-1 nanoparticles.

Diatomite is considered a good candidate for the preparation of hierarchically porous composites [24–31] because it occurs naturally and has a well-developed porosity. Diatomite, also known as diatomaceous earth or kieselgur, is a fossil assemblage of diatom shells composed of amorphous hydrated silica ($SiO_2 \cdot nH_2O$) and is classified as opal-A in mineralogy. It is characterized by a macroporous structure with pore sizes ranging from nanometers to micrometers [32–34]. As a fine-grained, low-density biogenetic sediment that is non-toxic and readily available in ton quantities at low cost, diatomite has been studied to evaluate its feasibility as a support for nanoparticle coating. Several reports have presented various preparation methods for zeolite nanoparticles coated onto diatomite. Anderson et al. [35,36] proposed a process involving ultrasonically loading silicalite-1 seeds onto diatomite, followed by a hydrothermal growth process of the seeds. The obtained composite showed a low specific surface area (S_{BET}, 29.2 m^2/g) and micropore volume ($V_{micropore}$, 0.01 cm^3/g). Wang et al. [28] proposed the layer-by-layer (LBL) zeolite deposition method in which silicalite-1 nanoparticles were assembled onto diatomite via electrostatic attraction. The resulting composite possessed an improved S_{BET} and $V_{micropore}$ of 44.0 m^2/g and 0.016 cm^3/g, respectively, but the loading amount of zeolite remained low, at 10%. To increase the zeolite loading amount, Wang et al. [29] then developed the LBL technique, and an effective vapor-phase transport (VPT) treatment was subsequently used to supplement the LBL procedure. The zeolite loading amount of the composite reached 51.4%, after a 10-day hydrothermal reaction and the composite also exhibited an excellent benzene adsorption capacity (46.0 mg/g). However, the extraordinarily long preparation period (more than 10 days) and laborious procedures constrain the industrial application of the synthesized adsorbent. In addition, the rigorously high temperature and pressure conditions required in the VPT treatment pose certain risks, making it less suitable for large-scale production. Thus, a facile synthesis method for silicalite-1 coating is urgently needed.

The VOC adsorption performance and industrial application of the adsorbents are typically evaluated in terms of the adsorption capacity, diffusion and mass transfer efficiency, and reusability. Adsorption capacity [37,38] has been recognized as the most common metric for testing the adsorption performance because of its ease of measurement, whereas the diffusion efficiency and reusability of adsorbents are rarely studied. Fletcher et al. [39,40] investigated the adsorption–desorption kinetics for vapors on activated carbon. Dou et al. [12] reported the mass transfer efficiency of benzene over carbon–silica composites. However, to date, few reports have systematically investigated the mass transfer efficiency of diatomite/zeolite composites, and there are no related reports regarding their reusability.

Therefore, the objective of this study is to develop a facile method for the preparation of a diatomite/silicaite-1 composite and to systematically assess the feasibility of applying such a novel synthesized adsorbent for the removal of VOCs. In the present study, silicalite-1 nanoparticles were synthesized in situ on the surface of the modified diatomite through a simple and mild low-temperature reflux reaction, yielding a diatomite/silicalite-1 composite with a high zeolite loading amount. Several techniques (X-ray diffraction, scanning electron microscopy, mercury intrusion tests and N$_2$ adsorption–desorption isotherms) were used to investigate the morphology and texture of the composite. Benzene was used as the model organic compound to systematically evaluate the adsorption–desorption performance of the obtained diatomite/silicalite-1 composite. Benzene, a typical VOC, is primarily released from building and decoration materials in indoor environments and leads to massive environmental problems in industrial and domestic settings [41,42]. In this work, the benzene adsorption capacity of the novel synthesized composite was studied. The diffusion and mass transfer kinetics and reusability were systematically investigated as well. A static benzene adsorption–desorption test was conducted using an accurate, intelligent gravimetric analyzer, and we adopted a method involving breakthrough

curves and experimental installations to evaluate the diffusion performance and reusability of the adsorbent.

2. Experimental

2.1. Reagents and materials

Tetraethoxysilane (TEOS, 99%) and poly(diallyldimethylammonium chloride) (PDDA, 20% aqueous solution), used as a silicon source for the zeolite synthesis solutions and the surface modifier of diatomite, respectively, were purchased from Aldrich. The template agent, tetrapropylammonium hydroxide (TPAOH, 25% aqueous solution), was provided by Zhejiang Kente Chemical Co. Raw diatomite powder (denoted as Dt) was obtained from the Changbai deposit in Jiling Province, China, and its chemical composition was determined by chemical analysis to be as follows: SiO_2, 86.18; Al_2O_3, 3.08; Fe_2O_3, 1.47; MgO, 0.33; CaO, 0.37; Na_2O, 0.05; K_2O, 0.51; MnO, 0.01; P_2O_5, 0.06; TiO_2, 0.17; and loss on ignition 8.56. Distilled water (18.2 ΩM cm) was used in all of the experiments. Commercial MFI-type high-silicon molecular sieves (denoted as ZSM-5) were purchased from Fuxu Molecular Sieve Co. All of the reagents and materials were used as received without any further treatment.

2.2. In situ synthesis of the diatomite/silicalite-1 composite

Fig. 1 shows the processing route for the synthesis of the diatomite/silicalite-1 composite. A zeolite precursor suspension with a $TEOS:TPAOH:H_2O$ molar ratio of 1:0.36:19.2 was prepared [43]. In this process, 32.6 ml of TPAOH (25% aqueous solution) was slowly added to 13.76 ml of distilled water, followed by the cautious dropwise addition of TEOS. The suspension was continuously stirred and incubated for 24 h at room temperature to allow full hydrolysis of the silicon source.

Prior to the synthesis, 3 g of Dt was submerged in 160 ml of a 0.5% PDDA solution, stirring vigorously for approximately 3 h to allow surface modification. It was then dried and mixed with the zeolite precursor suspension. The mixture was transferred to a beaker under heating reflux in a silicon oil bath at 101 °C for 72 h. The obtained solid was centrifuged (4000 rpm for 5 min) and rinsed with distilled water three or four times to remove the superfluous silicalite-1 nanoparticles. Then, the solid was dried at 80 °C overnight and subsequently calcined at 550 °C for 6 h. The final resulting sample was denoted as M-Dt/Sil-1$_{nano}$. Pure silicalite-1 nanoparticles without the addition of diatomite and the diatomite/silicalite-1 composite without pretreatment of diatomite were also prepared and are Sil-1$_{nano}$ and Dt/Sil-1$_{nano}$, respectively.

2.3. Characterization methods

X-ray diffraction (XRD) patterns were recorded on a Bruker D8 Advance diffractometer with a Ni filter and a Cu Kα radiation source (λ = 0.154 nm) operated under a generating voltage of 40 kV and a current of 40 mA. The diffractometer scanned at a rate of 3° (2θ)/min.

Scanning electron microscopy (SEM) images were obtained using a ZEISS Supra 55 field emission scanning electron microscope. Transmission electron microscopy (TEM) images were acquired using a JEOL JEM-2100 electron microscope operating at an acceleration voltage of 200 kV. The specimens were pretreated through the following procedure: the sample was ultrasonically dispersed in ethanol for 5 min, and then, a drop of the suspension was dropped onto a carbon-coated copper grid, which was left to stand for 10 min before being placed in the microscope.

Mercury intrusion tests to evaluate the macropore size distribution of the samples were conducted on a Micromeritics AutoPore IV 9500 porosimeter in the pressure range of 0.1–60,000 psi. A Micromeritics ASAP 2020 system was used to measure the N_2 adsorption–desorption isotherms at liquid nitrogen temperature (77 K). All of the samples were degassed at 300 °C under vacuum for 12 h before the measurement. The specific area (S_{BET}) was calculated from the N_2 adsorption data using the multi-point Brunauer–Emmett–Teller (BET) equation. The total pore volume (V_{total}) was determined at a relative pressure of ca. 0.99, and the micropore pore volume ($V_{micropore}$) was obtained via the HK
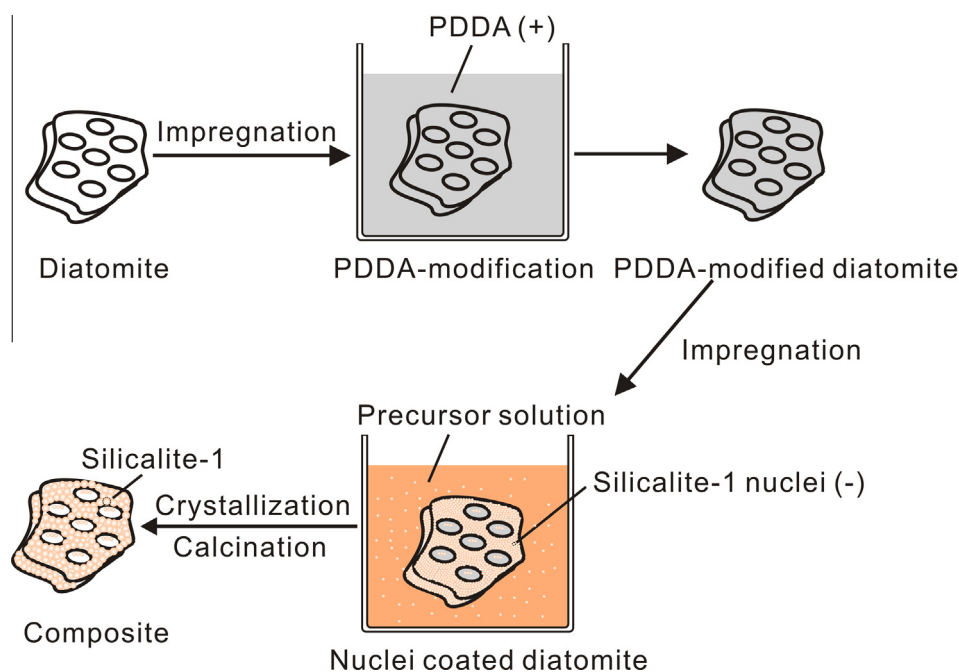

Fig. 1. Schematic diagram for the synthesis of the diatomite/silicalite-1 composite.

method. The micropore surface area ($S_{micropore}$) of the composite was evaluated using the *t*-plot method. The non-local density functional theory (NLDFT) model [44,45], which determines both the micropore and mesopore size distributions, was used to evaluate the hierarchically porous structure of the composite in the range of 0–20 nm.

2.4. Static benzene adsorption and desorption tests

The benzene adsorption–desorption equilibrium tests for various samples were conducted using an intelligent gravimetric analyzer (IGA-002, Hiden Isochema Instrument) with a sensitivity of 0.1 μg at room temperature (25 °C). The apparatus possesses an ultra-high vacuum system and can accurately control the subtle weight changes of the samples by changing the pressures [12]. Sample with a mass of 50 mg per run was heated at 300 °C for 12 h under vacuum before the start of the test to remove the impurities and avoid the adsorption of water. The static benzene adsorption capacity was recorded by altering the pressure until it approached the saturated vapor pressure.

2.5. Dynamic benzene adsorption measurements

The dynamic benzene adsorption and desorption performance was measured with a constant-flow method at a constant temperature (25 °C) using an instrument set-up equipped with an online gas chromatography device (GC), as shown in Fig. 2. Before the measurement, samples were degassed at 300 °C for 4 h to remove physically adsorbed water and other organic impurities, and the apparatus was purged with N_2 for 4 h. Then, 0.5 g of the sample was placed in the sample tube mounted on the adsorption reaction bed (Fig. 2). The total flow rate of benzene was controlled at 3 ml min^{-1} with a split ratio of 1:1. During the benzene adsorption process, organic benzene vapor carried by N_2 flowed through the sample tube and was adsorbed onto the sample. The residual concentration of benzene was recorded by a GC equipped with a flame ionization detector. After the reaction, the quartz tube containing the sample was heated again at 300 °C for 4 h, and the entire process was repeated 4 times to evaluate the reusability of the novel synthesized composite.

3. Results and discussion

3.1. Characterization of the M-Dt/Sil-1$_{nano}$ composite

Fig. 3 shows the XRD patterns of various samples. The XRD pattern of raw Dt is characterized by a broad peak centered at approximately 21.8° (2θ) with a *d*-spacing of 0.409 nm, revealing the main phase of amorphous opal-A, which corresponds to the literature [32]. The weak peak centered at 26.6° (2θ) is ascribed to the small
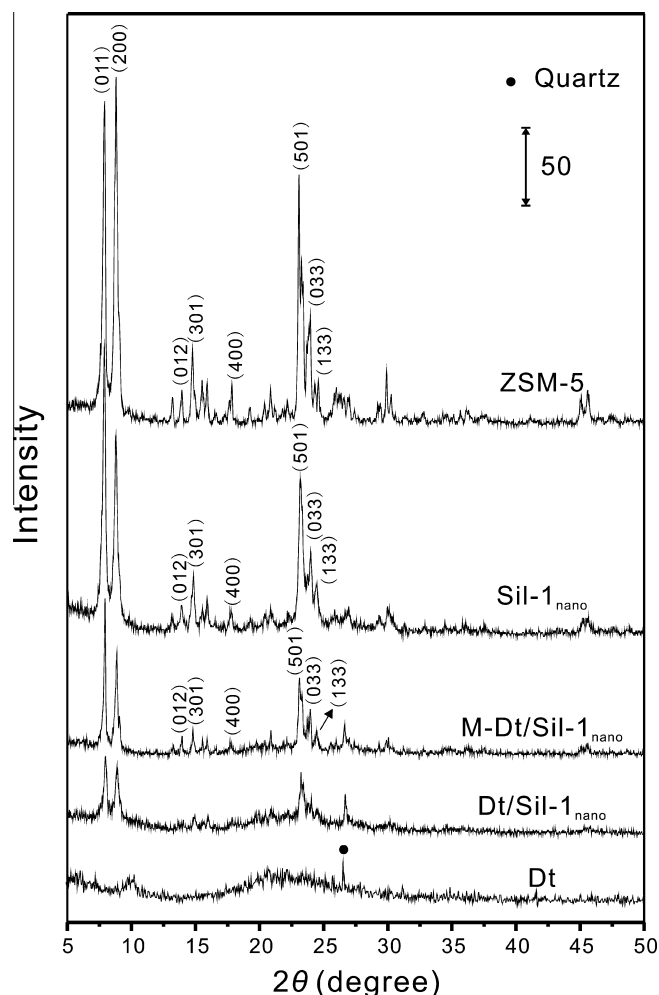
Fig. 2. Schematic diagram of the dynamic benzene adsorption instrument.

Fig. 3. XRD patterns of Dt, Dt/Sil-1$_{nano}$, M-Dt/Sil-1$_{nano}$, Sil-1$_{nano}$ and commercial ZSM-5.

quantity of quartz impurity (less than 4 wt% according to a semi-quantitative determination). The synthesized Sil-1$_{nano}$ and purchased commercial ZSM-5 (Fig. 3) consist mainly of crystalline MFI-type silicalite zeolite with peaks centered at 7.8°, 8.8°, 14.8°, 17.6°, 23°, 23.6°, and 24.4° (2θ), which are indexed as the (0 1 1), (2 0 0), (3 0 1), (4 0 0), (5 0 1), (0 3 3) and (1 3 3) reflections, respectively, based on Powder Diffraction File No. 44-0696. The broadened diffraction lines of Sil-1$_{nano}$ compared with commercial ZSM-5 (micrometer-sized particles) can likely be attributed to its synthetic nanometer-sized particles. The characteristic reflections of the MFI-type zeolitic structure appeared in the obtained M-Dt/Sil-1$_{nano}$ and were in accordance with that of Sil-1$_{nano}$, indicating the existence of silicalite-1 nanoparticles in the novel synthesized composite. Compared to Sil-1$_{nano}$, the relatively narrow diffraction lines of M-Dt/Sil-1$_{nano}$ are ascribed to the micron-sized particles of the diatomite, implying that the silicalite-1 nanoparticles successfully coat the support. In addition, the diffraction intensity of the M-Dt/Sil-1$_{nano}$ is lower than those of Sil-1$_{nano}$ and commercial ZSM-5, likely due to the lower zeolite content (compared with pure silicalite-1 nanoparticles) resulting from the coating process of silicalite-1 onto diatomite. The lower diffraction intensity of Dt/Sil-1$_{nano}$ (Fig. 3) compared to that of M-Dt/Sil-1$_{nano}$ indicates that the pretreatment of diatomite, the PDDA modification, facilitates the coating of silicalite-1 nanoparticles onto the diatomite surface.

As shown by the SEM images in Fig. 4a$_1$, the dominant diatoms of raw Dt, categorized as the *Coscinodiscus* Ehrenberg (*Centrales*),
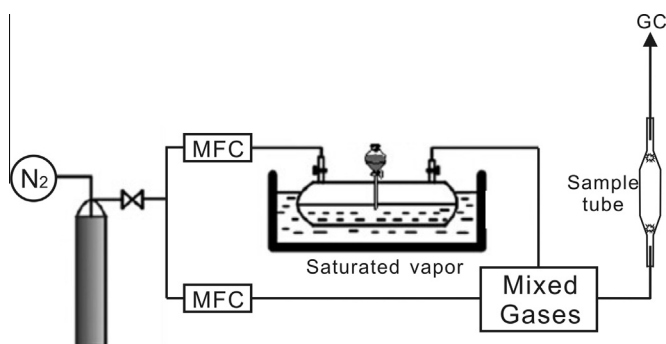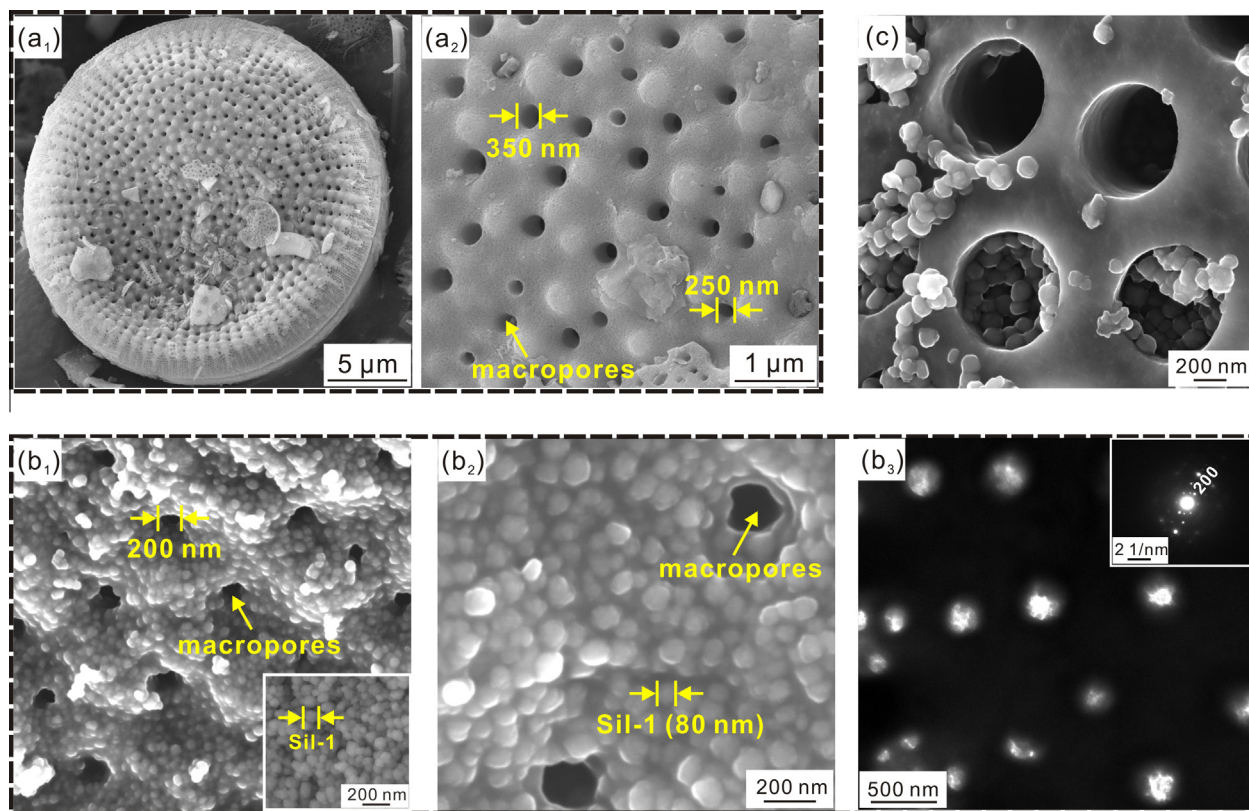
Fig. 4. SEM images of (a$_1$), (a$_2$) Dt; (b$_1$), (b$_2$) M-Dt/Sil-1$_{nano}$; and (c) Dt/Sil-1$_{nano}$; and TEM image of (b$_3$) M-Dt/Sil-1$_{nano}$.

are discshaped with highly developed macropores. Their macropore diameter (0.1–0.8 μm), varying regularly from the edge (100–250 nm) of the disc to the center (250–800 nm) was clearly observed at a higher magnification (Fig. 4a$_2$). The surface of the diatomite remained smooth without any impurity adhesions. The relatively uniform particle diameter (20–40 μm) and thickness (1.2–1.8 μm) of the diatom frustules were not visible in the SEM images. Fig. 4b$_1$ and b$_2$ provide the SEM images of the obtained M-Dt/Sil-1$_{nano}$ composite after the *in situ* coating process. The surface of Dt was coated with nanoparticles with particle sizes of 80 nm, which is in accordance with the particle sizes observed for the synthesized sphere-shaped Sil-1$_{nano}$, as shown in the insert of Fig. 4b$_1$. This result illustrates that the silicalite-1 nanoparticles were successfully coated on the surface of the diatomite. As observed at a higher magnification (Fig. 4b$_2$), the 80-nm silicalite-1 nanoparticles were entirely and homogeneously distributed on the surface of Dt, forming the M-Dt/Sil-1$_{nano}$ composite. The macropores of the M-Dt/Sil-1$_{nano}$ composite were clearly visible having pore sizes of 100–200 nm. The decreased central macropore sizes compared to those of the Dt support is ascribed to the fact that some silicalite-1 nanoparticles (80 nm) coated the inner walls of the central macropores. This result is in good agreement with the transmission electron microscope result in Fig. 4b$_3$, showing that the macropores of the Dt support were distinctly in the M-Dt/Sil-1$_{nano}$ composite with a layer of Sil-1$_{nano}$ coated on the inner edge of the pores. The inserted SEAD patterns of a crystal in Fig. 4b$_3$, matching the crystalline structure previously reported for MFI zeolite [46], further confirmed the coating of silicalite-1 nanoparticles onto diatomite.

The SEM image of the Dt/Sil-1$_{nano}$ composite without the pre-modification of the diatomite (Fig. 4c) revealed that only a small amount of silicalite-1 nanoparticles were inhomogeneously coated onto the diatomite, and the macropores of this support were nearly blocked by the nanoparticles. The complete and homogenous coating of silicalite-1 nanoparticles in M-Dt/Sil-1$_{nano}$ (Fig. 4b$_1$ and b$_2$) compared to that in Dt/Sil-1$_{nano}$ (Fig. 4c) is due to the pre-modification mechanism. That is, the surface of the diatomite was negatively charged [47–49] in the alkaline silicalite-1 precursor solutions (pH = 12.5), which allows a barrier between it and the negatively charged silicalite-1 nuclei to develop [50] during the pre-hydrolysis process because of the electrostatic repulsion, leading to large bare areas of diatomite with no silicalite-1 coating. In contrast, after PDDA modification, the surface charge of the diatomite changed from negative to positive [51] (Zeta potential value was shown in Supplementary Table S1), which is beneficial for the directional adhesion of the negatively charged silicalite-1 nuclei (Supplementary Table S1) resulting from electrostatic attraction. Thus, more silicalite-1 nuclei were dispersed onto diatomite, contributing to the following homogeneous *in situ* crystallization of the nuclei.

As shown in Fig. 5a, the typical N$_2$ adsorption–desorption isotherm of raw Dt featured type II curves with a minor H3 hysteresis loop according to the IUPAC classification [24], which indicates the existence of small quantities of mesopores in the Dt. The extremely small amount of N$_2$ adsorption at relatively low pressures ($P/P_0 \leqslant 0.1$) is caused by the filling of few micropores, and the rapidly increased adsorption quantities when $P/P_0 \approx 1.0$ suggest abundant macroporosity. This trend is in agreement with the SEM images (Fig. 4a$_2$), indicating that Dt possesses highly developed macropores. The Sil-1$_{nano}$ in Fig. 5b shows type IV adsorption–desorption isotherm curves with an evident H3 hysteresis loop, which is an indication of the formation of mesopores from the stacking voids of the Sil-1. The initial rapid increase in the amount of N$_2$ adsorption when $P/P_0 \leqslant 0.1$ followed by a mild stage is ascribed to the filling of the micropores by the nanoparticles, and the sharp increase in the adsorption quantity at $P/P_0 \approx 1.0$ is mainly due to the exter-
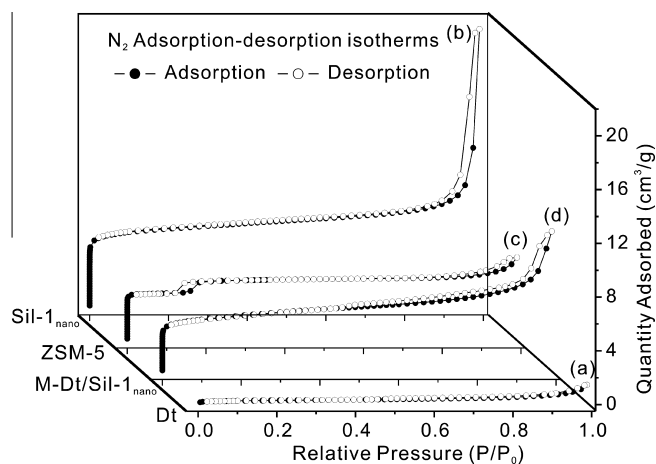
Fig. 5. N$_2$ adsorption–desorption isotherms of (a) Dt; (b) Sil-1$_{nano}$; (c) ZSM-5 and (d) M-Dt/Sil-1$_{nano}$.

nal adsorption caused by the agglomeration of silicalite-1 nanoparticles. The commercial ZSM-5 (Fig. 5c) exhibited similar adsorption–desorption isotherm curves with Sil-1$_{nano}$. The additional hysteresis loop appearing at $P/P_0 \approx 0.15$ reflects the formation of minor mesopores in the ZSM-5. The M-Dt/Sil-1$_{nano}$ composite in Fig. 5d displays the same type IV curves and H3 hysteresis loop as the Sil-1$_{nano}$ and ZSM-5. The steep increase in the amount of N$_2$ adsorption at $P/P_0 \leqslant 0.1$ suggests massive micropores in the composite corresponding to Sil-1$_{nano}$ and further demonstrates the coating of silicalite-1 nanoparticles onto diatomite. However, the hysteresis loop of the M-Dt/Sil-1$_{nano}$ composite ($P/P_0 \approx 0.4$) is larger than that of Sil-1$_{nano}$ ($P/P_0 \approx 0.6$), implying a more extensive mesoporous distribution of the composite. Moreover, the gradual increase in the amount of N$_2$ adsorption when P/P_0 approaches 1.0 compared to that of Sil-1$_{nano}$ is ascribed to the alleviated agglomeration of the silicalite-1 nanoparticles resulting from the surface coating process, improving the dispersity of the nanoparticles, which may facilitate VOC adsorption.

The microporous and mesoporous size distributions of various samples calculated from the NLDFT method [45] are illustrated in Fig. 6a. The major population centered at 0.6 nm, which occurred in all samples, is attributed to the inherent micropores of the MFI-type zeolite. The small population centered at 1.2 nm in Sil-1$_{nano}$ and M-Dt/Sil-1$_{nano}$ is ascribed to the stacking voids of the smaller silicatite-1 nanoparticles. The only significant population centered at 2.9 nm is assigned to the mesopores in ZSM-5, which is in good agreement with the additional hysteresis loop in the N$_2$ adsorption–desorption isotherm curves (Fig. 5c), indicating the formation of minor mesopores. Mesoporous populations centered at 13.1 and 16.8 nm in Sil-1$_{nano}$ are attributed to the stacking voids of larger silicalite-1 nanoparticles. The broader mesoporous size distributions for M-Dt/Sil-1$_{nano}$ compared to those of Sil-1$_{nano}$ and ZSM-5, with additional mesoporous populations centered at 2–6, 10.4, 13.1 and 16.8 nm respectively, are due to the alleviated agglomeration and improved dispersity of the Sil-1$_{nano}$ nanoparticles via the in situ coating synthesis onto the diatomite supports.

The mercury intrusion results displayed in Fig. 6b reflect the macroporous size distributions of the Dt and M-Dt/Sil-1$_{nano}$ composite. The macropore populations centered at 0.14, 0.23 and 0.7 μm, respectively are ascribed to the intrinsically macroporous structure of Dt, and the 3.2 μm population belongs to the stacking macroporous voids of the diatom shells. For the M-Dt/Sil-1$_{nano}$ composite, the macropore populations centered at 0.28 and 0.43 μm indicate that the macroporosity is maintained in the Dt. The disappeared or reduced macropore populations of the Dt

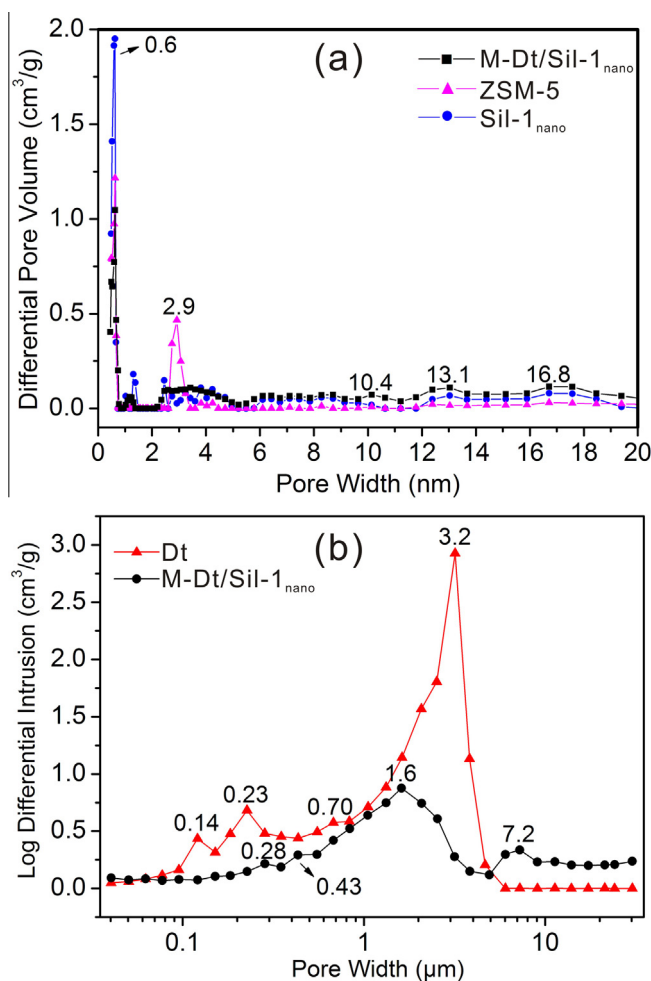Fig. 6. (a) Microporous and mesoporous size distributions of Sil-1$_{nano}$, ZSM-5 and M-Dt/Sil-1$_{nano}$; (b) macroporous size distributions of Dt and M-Dt/Sil-1$_{nano}$.

support in M-Dt/Sil-1$_{nano}$ suggest a decrease in the inherent macropores of the Dt support, which likely results from a diminishment of the macroporous space as the silicalite-1 nanoparticles (80 nm) coat the internal surface of the Dt support. The macropore populations centered at 1.6 and 7.2 μm are attributed to the stacking voids following the coating with silicalite-1. The pore size distribution results indicate that the resulting M-Dt/Sil-1$_{nano}$ composite possesses hierarchically porous structures, inherent micropores and stacking mesopores from the silicalite-1 nanoparticles, and the inherent and stacking macropores from the diatomite support. These results indicate the possibility of a favorable mass transfer performance because of the introduction of a macroporous structure in the composite.

As the silicalite-1 nanoparticles were introduced into the composite in the in situ coating process, the S_{BET} and $V_{micropore}$ values of the M-Dt/Sil-1$_{nano}$ composite (348.7 m^2/g and 0.127 cm^3/g, respectively, Table 1) are noticeably higher than those of raw Dt (24.0 m^2/g and 0.009 cm^3/g). The slightly higher S_{BET} and $V_{micropore}$ values of the M-Dt/Sil-1$_{nano}$ compared to those of commercial micron-sized ZSM-5 (330.7 m^2/g and 0.124 cm^3/g, respectively, Table 1) are attributed to the nano-sized silicalite-1 coated onto diatomite. The $S_{micropore}$ of the M-Dt/Sil-1$_{nano}$ composite (163.6 m^2/g, Table 1) calculated from the t-plot surface area is lower than that of ZSM-5 (273.7 m^2/g) and Sil-1$_{nano}$ (302.5 m^2/g), which is ascribed to the certain amount of zeolite loading on the composite compared with the pure zeolites. However, the $S_{external}$ of the composite, as listed

Table 1
N₂ adsorption–desorption results for Dt, M-Dt/Sil-1$_{nano}$, Dt/Sil-1$_{nano}$, ZSM-5 and Sil-1$_{nano}$.

Sample	S_{BET}/m² g⁻¹	$S_{micropore}$[a]/m² g⁻¹	$S_{external}$[a]/m² g⁻¹	V_{total}/cm³ g⁻¹	$V_{micropore}$[b]/cm³ g⁻¹	$W_{zeolite}$[c] (%)
Dt	24.0	4.3	20.2	0.051	0.009	–
M-Dt/Sil-1$_{nano}$	348.7	163.6	185.1	0.365	0.127	60.2
Dt/Sil-1$_{nano}$	186.9	73.4	113.5	0.176	0.072	32.1
ZSM-5	330.7	273.7	57.8	0.216	0.124	100
Sil-1$_{nano}$	503.3	302.5	207.3	0.720	0.196	100

$W_{zeolite}$% = [$V_{micropore}$ (composite) − $V_{micropore}$ (Dt)] × 100%/$V_{micropore}$ (Sil-1$_{nano}$).

[a] $S_{micropore}$ was calculated from the *t*-plot surface area, and $S_{external}$ was calculated from the S_{BET} and $S_{micropore}$ using the equation $S_{external}$ = S_{BET} − $S_{micropore}$.

[b] The micropore volume, $V_{micropore}$, was determined using the HK method.

[c] The wt% of zeolite in the composites was calculated from the micropore volumes using the equation.

in Table 1, is higher than that for ZSM-5 and is similar to Sil-1$_{nano}$, indicating the improved dispersity of the composite. The S_{BET} and $V_{micropore}$ values of the M-Dt/Sil-1$_{nano}$ composite are also considerably higher than those of Dt/Sil-1$_{nano}$ (186.9 m²/g and 0.072 cm³/g), which is a result of more silicalite-1 nanoparticles coated onto the diatomite via the PDDA modification pre-treatment. This is consistent with the SEM results showing that large bare areas of diatomite existed in Dt/Sil-1$_{nano}$ (Fig. 4c) as well as with the considerably higher amount of zeolite loading on the M-Dt/Sil-1$_{nano}$ (60.2%) than on the Dt/Sil-1$_{nano}$ (32.1%, Table 1). Notably, the amount of zeolite loading on the M-Dt/Sil-1$_{nano}$ composite is approximately 6 times higher than that on the diatomite/MFI-type zeolite composite reported by Wang et al. (10%) [28] and even higher than the composite synthesized using a 10-day hydrothermal method (51.2%) [29]. This higher amount of loading can be ascribed to the superiority of the *in situ* coating process versus the conventional LBL deposition technique. The electrostatic attraction between modified diatomite and smaller amorphous silicalite-1 nuclei (10–20 nm, tested in our previous study) [52] in the *in situ* coating process is stronger than that between diatomite and crystalline silicalite-1 nanoparticles (80 nm), facilitating the attraction of nuclei to the diatomite surface to reach a charge balance and leading to the improved homogeneity of the resulting M-Dt/Sil-1$_{nano}$ composite in the following crystallization process. The advantageously higher zeolite utilization efficiency of the M-Dt/Sil-1$_{nano}$ synthesized through a facile *in situ* method implies a higher VOC removal efficiency in the novel composite.

3.2. Benzene adsorption performance of the M-Dt/Sil-1$_{nano}$ composite

3.2.1. Static benzene adsorption isotherms of the composite

Fig. 7 shows the static benzene adsorption isotherms of various samples at room temperature (25 °C). The benzene adsorption isotherm of raw Dt is type II with a small hysteresis loop, which is in good agreement with the N₂ adsorption–desorption isotherms in Fig. 5a, indicating the limited number of micropores existing in Dt. Raw Dt displayed an extremely low benzene adsorption equilibrium capacity with a value of 1.0 mg/g, which results from that of Dt. The uptake of such small benzene molecules only depends on disordered diffusion because of its macroporosity with a low $V_{micropore}$ (0.009 cm³/g), leading to the low adsorption capacity. Both the Sil-1$_{nano}$ and ZSM-5 in Fig. 7 exhibited type I benzene adsorption isotherms. The initial rapidly increasing amount of benzene adsorption at low absolute pressures (less than 10 mbar) is attributed to the microporous filling of benzene molecules caused primarily by their inherent micropores. The steadily increasing amount of benzene adsorption under absolute pressures exceeding 20 mbar is ascribed to the stacking mesoporous filling of the benzene molecules. Because of the external adsorption caused by an agglomeration of the nanoparticles, the Sil-1$_{nano}$ showed a steeper adsorption trend than ZSM-5 when the absolute pressure
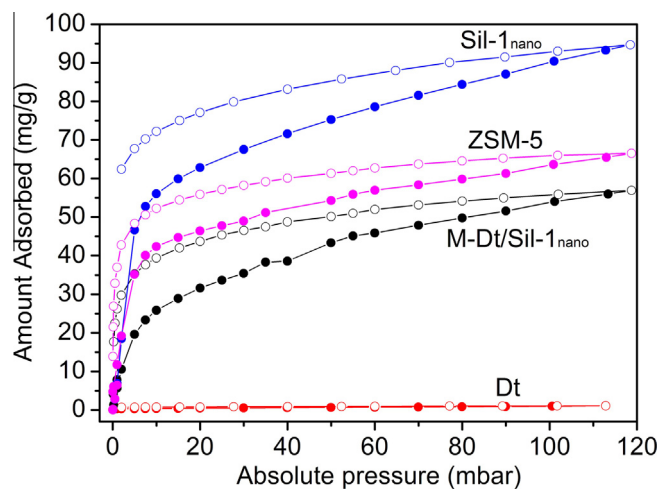

Fig. 7. Static benzene adsorption–desorption isotherms of various samples.

approached 120 mbar. The static equilibrium capacities of Sil-1$_{nano}$ and ZSM-5 for the adsorption of benzene are 94.7 and 66.5 mg/g, respectively. The M-Dt/Sil-1$_{nano}$ composite exhibited type IV adsorption isotherm curves, and the benzene amount increased steadily throughout the adsorption process. The flatter adsorption curves of the M-Dt/Sil-1$_{nano}$ composite compared to those of Sil-1$_{nano}$ and ZSM-5 are attributed to the enhanced dispersity of the nanoparticles resulting from the Sil-1$_{nano}$ nanoparticle coating the diatomite and forming a hierarchically porous structure, which contributes to the steady increase in the amount of benzene adsorbed. M-Dt/Sil-1$_{nano}$ possessed a static benzene adsorption capacity of 57.1 mg/g, substantially exceeding that of the diatomite/silicalite-1 composites prepared by Wang et al. (46.0 mg/g) [29]. This higher capacity is achieved because the pre-modification *in situ* coating route facilitates the alleviation of the agglomeration problem and increases in the loading amount of the silicalite-1 nanoparticles compared with the conventional LBL technique. Considering the zeolite loading amount of 60.2%, the normalized static benzene adsorption capacity of the composite per unit mass of zeolite reached 94.9 mg/g (Sil-1$_{nano}$), which is considerably higher than that of commercial ZSM-5 and slightly higher than that of Sil-1$_{nano}$, indicating the excellent static benzene adsorption capacity of the novel synthesized M-Dt/Sil-1$_{nano}$ composite.

3.2.2. Dynamic benzene adsorption behaviors of the composite

The breakthrough measurements are described as intuitive reflections of the dynamic performances of the adsorbents in a continuous VOC adsorption process [53]. The breakthrough curves for all samples are shown in Fig. 8, and these curves were fitted
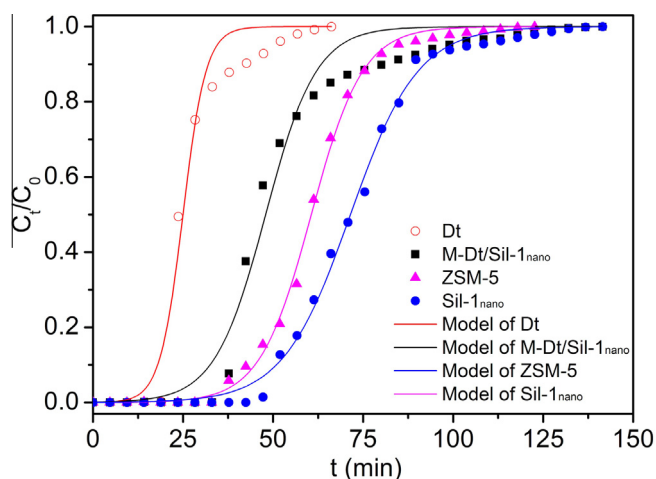
Fig. 8. Breakthrough curves of Dt, M-Dt/Sil-1$_{nano}$, ZSM-5 and Sil-1$_{nano}$ for benzene adsorption.

using the Yoon and Nelson model based on the following equation [54]:

$$t = \tau + 1/k[C_t/(C_0 - C_t)] \tag{1}$$

where t is the breakthrough time, C_0 and C_t (mmol/L) are the initial injected benzene concentration and detected effluent benzene concentration adsorbed at time t respectively, C_t/C_0 reflects the relative benzene concentration variations during the breakthrough process, τ is the time when the breakthrough concentration reaches half of the initial concentration ($C_t = 0.5C_0$), and k is the rate constant determined by the diffusion and mass transfer characteristics.

The dynamic benzene adsorption capacities (q, mg/g) of various samples calculated by the integration of the surface areas from the acquired breakthrough curves were based on the following equation [55,56]:

$$q = M/(1000m_1) \int_{t_1}^{t_2} F(C_0 - C_t)dt \tag{2}$$

where M (g/mol) is the molecular mass of benzene, m_1 (g) is the initial weight of the adsorbents before the test, t_1 (min) is the breakthrough time without the column, t_2 (min) is the breakthrough time with the packed column, and F (mL/min) represents the N_2 flow rate. The dead space was obtained by running blanks without the column.

A longer breakthrough time for the adsorbent in the VOC adsorption process typically indicates a higher dynamic capacity [57,58]. As shown in Fig. 8, all of the curves increased sharply over time with the breakthrough time decreasing in the order of Dt (~19 min) < M-Dt/Sil-1$_{nano}$ (~28 min) < ZSM-5 (~38 min) < Sil-1$_{nano}$ (~47 min). Therefore, the dynamic benzene adsorption capacities follow the order of Sil-1$_{nano}$ > ZSM-5 > M-Dt/Sil-1$_{nano}$ > Dt, correlating well with the dynamic benzene adsorption capacity values shown in Table 2. This result is in good agreement with the $V_{micropore}$ values of these samples in Table 1, suggesting that the microporous filling of the benzene molecules is a considerable critical step in the adsorption process. However, M-Dt/Sil-1$_{nano}$ showed a lower dynamic adsorption capacity (148.1 mg/g) than the commercial ZSM-5 (173.9 mg/g) despite having a higher $V_{micropore}$ value. This result is likely due to the appearance of abundant mesopores (2.9 nm) approaching the microporous region, thus providing similar openings for benzene molecules. Regarding the zeolite loading amount of the M-Dt/Sil-1$_{nano}$ composite of 60.2%, the normalized dynamic benzene adsorption capacity of the composite (q_s, mg/g) reached 246.0 mg/g, which is considerably higher than those of commercial ZSM-5 (173.9 mg/g) and Sil-1$_{nano}$ (207.7 mg/g) in accordance with the results of the static benzene adsorption capacity (Fig. 7), thus indicating the higher zeolite utilization efficiency of the novel synthesized composite. In the composite, silicalite-1 nanoparticles are dispersed on the surface of the diatomite support, which improves their dispersity and stability, and provides a higher probability of obtaining full contact between the nanoparticles and benzene molecules. Such full contact enables a higher zeolite utilization efficiency for the composite than for pure Sil-1$_{nano}$ because of the alleviation of agglomeration of the nanoparticles.

The post-breakthrough curve of the M-Dt/Sil-1$_{nano}$, as shown in Fig. 8, is considerably shorter than those of ZSM-5 and Sil-1$_{nano}$, implying a lower mass transfer resistance and a superior diffusion behavior for the synthesized composite. These improvements are due to the introduction of macroporosity in the M-Dt/Sil-1$_{nano}$ composite from the Dt, as already indicated by the macropore size distribution in Fig. 6b, resulting in a reduction in the mass transfer resistance and facilitating the diffusion rate for gas penetration. Furthermore, the improved dispersity of the silicalite-1 nanoparticles via the coating process onto Dt provides more pathways for benzene molecules, promoting a rapid breakthrough process. The parameters of the Yoon and Nelson model are listed in Table 2. The rate constant value of the M-Dt/Sil-1$_{nano}$ composite (0.143 min^{-1}) is higher than those of commercial ZSM-5 (0.140 min^{-1}) and Sil-1$_{nano}$ (0.107 min^{-1}), and the post-breakthrough time at $C_t = 0.5C_0$ of the composite (47.93 min) is shorter than those of commercial ZSM-5 (60.62 min) and Sil-1$_{nano}$ (71.48 min). These results further demonstrate the remarkable diffusion and mass transfer performance of the novel synthesized composite for benzene adsorption.

3.2.3. Reusability of the composite for benzene adsorption

The evaluation for the cycling ability of the adsorbent is an important factor for industrial applications. The breakthrough
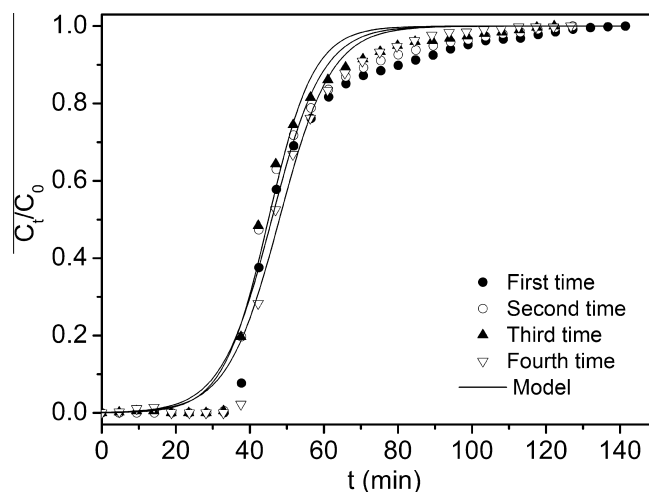
Fig. 9. Benzene adsorption breakthrough curves of the M-Dt/Sil-1$_{nano}$ composite cycled 4 times.

Table 2
The Yoon and Nelson equation parameters for Dt, M-Dt/Sil-1$_{nano}$, ZSM-5 and Sil-1$_{nano}$.

Sample	q (mg/g)	q_s (mg/g)	k (min^{-1})	τ (min)	R^2
Dt	73.7	–	0.313	24.98	0.976
M-Dt/Sil-1$_{nano}$	148.1	246.0	0.143	47.93	0.980
ZSM-5	173.9	173.9	0.140	60.62	0.998
Sil-1$_{nano}$	207.7	207.7	0.107	71.48	0.997

Table 3
Yoon and Nelson equation parameters for various cycles.

Cycles	q (mg/g)	q_s (mg/g)	k (min^{-1})	τ (min)	R^2	Efficiency (%)
First	148.1	246.0	0.143	47.93	0.980	–
Second	139.7	232.1	0.146	45.89	0.983	94.3
Third	135.2	224.6	0.163	45.00	0.987	91.3
Fourth	143.4	238.2	0.143	47.93	0.990	96.8

process of benzene adsorption over the novel M-Dt/Sil-1$_{nano}$ composite was conducted 4 times (Fig. 9). The fitting parameters of these 4 cycles are presented in Table 3. The overlapping fitted breakthrough curves of the composite presented good reproducibility over 4 cycles of benzene adsorption (Fig. 9), and the recycling efficiency of the composite for benzene adsorption remained relatively steady, exceeding 90% according to the integral of the curves from the baseline [31,54]. The diffusion and mass transfer properties of the M-Dt/Sil-1$_{nano}$ composite did not change significantly, as indicated by the slightly increased diffusion rate constants and constant τ values, thus demonstrating the promising industrial application prospects of the novel synthesized diatomite/silicalite-1 composite.

4. Conclusions

In this study, a hierarchically porous diatomite/silicalite-1 composite for VOC removal was prepared using a facile pre-modification *in situ* coating process, resulting in a coating of silicalite-1 nanoparticles on diatomite with a zeolite loading amount of up to 60.2%. The diatomite/silicalite-1 composite possessed a hierarchically porous structure with considerably higher S_{BET} and $V_{micropore}$ values than for the diatomite/MFI-type zeolite composite reported in previous studies. The prepared diatomite/silicalite-1 composite exhibited a considerably higher static benzene adsorption capacity and an enhanced benzene diffusion performance compared to those of pure synthesized silicalite-1 nanoparticles (Sil-1$_{nano}$) and commercial ZSM-5. The breakthrough curve results indicate that the composite displayed a lower mass transfer resistance and considerably faster penetration rate than Sil-1$_{nano}$ and commercial ZSM-5, arising from the macroporosity in the composite reducing the resistance to gas penetration. The improved dispersity of the silicalite-1 nanoparticles provides more pathways for the benzene molecules. The diffusion and mass transfer properties of the composite remained relatively steady after 4 adsorption cycles. With its facile preparation, meaningful benzene adsorption performance, and high reusability, this novel adsorbent, which can be easily scaled for industrial production, is a suitable candidate for the control of VOC emissions in industrial applications.

Acknowledgments

Appendix A. Supplementary data

Supplementary data associated with this article can be found, in the online version, at http://dx.doi.org/10.1016/j.cej.2016.02.099.

References

[1] A. Anfruns, M.J. Martin, M.A. Montes-Morán, Removal of odourous VOCs using sludge-based adsorbents, Chem. Eng. J. 166 (2011) 1022–1031.

[2] Q. Hu, J.J. Li, Z.P. Hao, L.D. Li, S.Z. Qiao, Dynamic adsorption of volatile organic compounds on organofunctionalized SBA-15 materials, Chem. Eng. J. 149 (2009) 281–288.

[3] K.J. Kim, H.G. Ahn, The effect of pore structure of zeolite on the adsorption of VOCs and their desorption properties by microwave heating, Microporous Mesoporous Mater. 152 (2012) 78–83.

[4] R.J. Weber, A.P. Sullivan, R.E. Peltier, A. Russell, B. Yan, M. Zheng, J. De Gouw, C. Warneke, C. Brock, J.S. Holloway, A study of secondary organic aerosol formation in the anthropogenic-influenced southeastern United States, J. Geophys. Res. Atmos. 112 (2007) (1984–2012).

[5] V. Blasin-Aubé, J. Belkouch, L. Monceaux, General study of catalytic oxidation of various VOCs over La$_{0.8}$Sr$_{0.2}$MnO^{3+x} perovskite catalyst—influence of mixture, Appl. Catal. B. Environ. 43 (2003) 175–186.

[6] F. Qu, L.Z. Zhu, K. Yang, Adsorption behaviors of volatile organic compounds (VOCs) on porous clay heterostructures (PCH), J. Hazard. Mater. 170 (2009) 7–12.

[7] M. Peng, L.M. Vane, S.X. Liu, Recent advances in VOCs removal from water by pervaporation, J. Hazard. Mater. 98 (2003) 69–90.

[8] C. Kennes, M.C. Veiga, Fungal biocatalysts in the biofiltration of VOC-polluted air, J. Biotechnol. 113 (2004) 305–319.

[9] F. Gironi, V. Piemonte, VOCs removal from dilute vapour streams by adsorption onto activated carbon, Chem. Eng. J. 172 (2011) 671–677.

[10] N.J. Foley, K.M. Thomas, P.L. Forshaw, D. Stanton, P.R. Norman, Kinetics of water vapor adsorption on activated carbon, Langmuir 13 (1997) 2083–2089.

[11] A.J. Fletcher, K.M. Thomas, Adsorption and desorption kinetics of *n*-octane and *n*-nonane vapors on activated carbon, Langmuir 15 (1999) 6908–6914.

[12] B.J. Dou, J.J. Li, Y.F. Wang, H.L. Wang, C.Y. Ma, Z.P. Hao, Adsorption and desorption performance of benzene over hierarchically structured carbon–silica aerogel composites, J. Hazard. Mater. 196 (2011) 194–200.

[13] S.K. Wirawan, D. Creaser, CO$_2$ adsorption on silicalite-1 and cation exchanged ZSM-5 zeolites using a step change response method, Microporous Mesoporous Mater. 91 (2006) 196–205.

[14] P. Monneyron, M.H. Manero, J.N. Foussard, Measurement and modeling of single-and multi-component adsorption equilibria of VOC on high-silica zeolites, Environ. Sci. Technol. 37 (2003) 2410–2414.

[15] R. Krishna, D. Paschek, Molecular simulations of adsorption and siting of light alkanes in silicalite-1, PCCP 3 (2001) 453–462.

[16] W.C. Li, A.H. Lu, R. Palkovits, W. Schmidt, B. Spliethoff, F. Schüth, Hierarchically structured monolithic silicalite-1 consisting of crystallized nanoparticles and its performance in the Beckmann rearrangement of cyclohexanone oxime, J. Am. Chem. Soc. 127 (2005) 12595–12600.

[17] A.J. Burggraaf, Z.A.E.P. Vroon, K. Keizer, H. Verweij, Permeation of single gases in thin zeolite MFI membranes, J. Membr. Sci. 144 (1998) 77–86.

[18] X.H. Gu, J.H. Dong, T.M. Nenoff, D.E. Ozokwelu, Separation of p-xylene from multicomponent vapor mixtures using tubular MFI zeolite membranes, J. Membr. Sci. 280 (2006) 624–633.

[19] G.E. Romanos, T.A. Steriotis, E.S. Kikkinides, N.K. Kanellopoulos, V. Kasselouri, J. D. Ramsay, P. Langlois, S. Kallus, Innovative methods for preparation and testing of Al$_2$O$_3$ supported silicalite-1 membranes, J. Eur. Ceram. Soc. 21 (2001) 119–126.

[20] X.F. Zhang, H.O. Liu, K.L. Yeung, Influence of seed size on the formation and microstructure of zeolite silicalite-1 membranes by seeded growth, Mater. Chem. Phys. 96 (2006) 42–50.

[21] G.T. Mabande, G. Pradhan, W. Schwieger, M. Hanebuth, R. Dittmeyer, T. Selvam, A. Zampieri, H. Baser, R. Herrmann, A study of silicalite-1 and Al-ZSM-5 membrane synthesis on stainless steel supports, Microporous Mesoporous Mater. 75 (2004) 209–220.

[22] A. Berenguer-Murcia, J. García-Martínez, D. Cazorla-Amorós, A. Linares-Solano, A.B. Fuertes, Silicalite-1 membranes supported on porous carbon discs, Microporous Mesoporous Mater. 59 (2003) 147–159.

[23] A. Zampieri, P. Colombo, G.T. Mabande, T. Selvam, W. Schwieger, F. Scheffler, Zeolite coatings on microcellular ceramic foams: a novel route to microreactor and microseparator devices, Adv. Mater. 16 (2004) 819–823.

[24] P. Yuan, D. Liu, M.D. Fan, D. Yang, R.L. Zhu, F. Ge, J.X. Zhu, H.P. He, Removal of hexavalent chromium [Cr(VI)] from aqueous solutions by the diatomite-supported/unsupported magnetite nanoparticles, J. Hazard. Mater. 173 (2010) 614–621.

[25] Z. Cherkezova-Zheleva, M. Shopska, I. Mitov, G. Kadinov, Size-dependent effects in supported highly dispersed Fe$_2$O$_3$ catalysts, doped with Pt and Pd, Hyperfine Interact. 198 (2010) 195–210.

[26] X.H. Liu, C.Y. Yang, Y.Q. Wang, Y.L. Guo, Y. Guo, G.Z. Lu, Effect of the diatomite pretreatment on the catalytic performance of TS-1/diatomite for toluene hydroxylation by H$_2$O$_2$ in fixed-bed reactor, Chem. Eng. J. 243 (2014) 192–196.

[27] S.F. Guo, L. Shi, Synthesis of succinic anhydride from maleic anhydride on Ni/diatomite catalysts, Catal. Today 212 (2013) 137–141.

[28] Y.J. Wang, Y. Tang, X.D. Wang, A.G. Dong, W. Shan, Z. Gao, Fabrication of hierarchically structured zeolites through layer-by-layer assembly of zeolite nanocrystals on diatom templates, Chem. Lett. (2001) 1118–1119.

[29] Y.J. Wang, Y. Tang, A. Dong, X. Wang, N. Ren, Z. Gao, Zeolitization of diatomite to prepare hierarchical porous zeolite materials through a vapor-phase transport process, J. Mater. Chem. 12 (2002) 1812–1818.

[30] J. Lu, F. Xu, W.M. Cai, Adsorption of MTBE on nano zeolite composites of selective supports, Microporous Mesoporous Mater. 108 (2008) 50–55.

[31] W.B. Yu, P. Yuan, D. Liu, L.L. Deng, W.W. Yuan, B. Tao, H.F. Cheng, F.R. Chen, Facile preparation of hierarchically porous diatomite/MFI-type zeolite composites and their performance of benzene adsorption: the effects of NaOH etching pretreatment, J. Hazard. Mater. 285 (2015) 173–181.

[32] P. Yuan, D. Liu, D.Y. Tan, K.K. Liu, H.G. Yu, Y.H. Zhong, A.H. Yuan, W.B. Yu, H.P. He, Surface silylation of mesoporous/macroporous diatomite (diatomaceous earth) and its function in Cu (II) adsorption: the effects of heating pretreatment, Microporous Mesoporous Mater. 170 (2013) 9–19.

[33] W.B. Yu, L.L. Deng, P. Yuan, D. Liu, W.W. Yuan, F.R. Chen, Preparation of hierarchically porous diatomite/MFI-type zeolite composites and their performance for benzene adsorption: the effects of desilication, Chem. Eng. J. 270 (2015) 450–458.

[34] D. Liu, P. Yuan, D.Y. Tan, H.M. Liu, M.D. Fan, A.H. Yuan, J.X. Zhu, H.P. He, Effects of inherent/enhanced solid acidity and morphology of diatomite templates on the synthesis and porosity of hierarchically porous carbon, Langmuir 26 (2010) 18624–18627.

[35] S.M. Holmes, C. Markert, R.J. Plaisted, J.O. Forrest, J.R. Agger, M.W. Anderson, C.S. Cundy, J. Dwyer, A novel method for the growth of silicalite membranes on stainless steel supports, Chem. Mater. 11 (1999) 3329–3332.

[36] M.W. Anderson, S.M. Holmes, N. Hanif, C.S. Cundy, Hierarchical pore structures through diatom zeolitization, Angew. Chem. 112 (2000) 2819–2822.

[37] T. Ben, H. Ren, S. Ma, D. Cao, J. Lan, X. Jing, W. Wang, J. Xu, F. Deng, J.M. Simmons, Targeted synthesis of a porous aromatic framework with high stability and exceptionally high surface area, Angew. Chem. 121 (2009) 9621–9624.

[38] Q. Hu, B.J. Dou, H. Tian, J.J. Li, P. Li, Z.P. Hao, Mesoporous silicalite-1 nanospheres and their properties of adsorption and hydrophobicity, Microporous Mesoporous Mater. 129 (2010) 30–36.

[39] A.J. Fletcher, Y. Yüzak, K.M. Thomas, Adsorption and desorption kinetics for hydrophilic and hydrophobic vapors on activated carbon, Carbon 44 (2006) 989–1004.

[40] A.J. Fletcher, Y. Uygur, K.M. Thomas, Role of surface functional groups in the adsorption kinetics of water vapor on microporous activated carbons, J. Phys. Chem. C 111 (2007) 8349–8359.

[41] D.J. Paustenbach, R.D. Bass, P. Price, Benzene toxicity and risk assessment, 1972–1992: implications for future regulation, Environ. Health Perspect. 101 (1993) 177.

[42] D. Ross, D. Siegel, D.G. Schattenberg, X.M. Sun, J.L. Moran, Cell-specific activation and detoxification of benzene metabolites in mouse and human bone marrow: identification of target cells and a potential role for modulation of apoptosis in benzene toxicity, Environ. Health Perspect. 104 (1996) 1177.

[43] P.J. Sterte, L.B. Tosheva, V.P. Valtchev, S.I. Mintova, Macrostructures of porous inorganic material and process for their preparation, US 6908604 B2 (2005).

[44] P.I. Ravikovitch, A.V. Neimark, Density functional theory model of adsorption deformation, Langmuir 22 (2006) 10864–10868.

[45] C. Vakifahmetoglu, Zeolite decorated highly porous acicular calcium silicate ceramics, Ceram. Int. 40 (2014) 11925–11932.

[46] G. Bonilla, I. Díaz, M. Tsapatsis, H.K. Jeong, Y. Lee, D.G. Vlachos, Zeolite (MFI) crystal morphology control using organic structure-directing agents, Chem. Mater. 16 (2004) 5697–5705.

[47] Y.X. Yang, J.D. Wu, Z.L. Huang, R.S. Chen, A.B. Dai, A study on surface electrochemical properties of several siatomites, J. Inorg. Chem. Nanjing 13 (1997) 11–15.

[48] G.V. Franks, Zeta potentials and yield stresses of silica suspensions in concentrated monovalent electrolytes: isoelectric point shift and additional attraction, J. Colloid Interface Sci. 249 (2002) 44–51.

[49] P.L. He, N.F. Hu, J.F. Rusling, Driving forces for layer-by-layer self-assembly of films of SiO$_2$ nanoparticles and heme proteins, Langmuir 20 (2004) 722–729.

[50] L. Tosheva, V.P. Valtchev, Nanozeolites: synthesis, crystallization mechanism, and applications, Chem. Mater. 17 (2005) 2494–2513.

[51] A. Panáček, A. Balzerová, R. Prucek, V. Ranc, R. Večeřová, V. Husičková, J. Pechoušek, J. Filip, R. Zbořil, L. Kvítek, Preparation, characterization and antimicrobial efficiency of Ag/PDDA-diatomite nanocomposite, Colloids Surf. B Biointerfaces 110 (2013) 191–198.

[52] W.W. Yuan, P. Yuan, D. Liu, W.B. Yu, L.L. Deng, F.R. Chen, Novel hierarchically porous nanocomposites of diatomite-based ceramic monoliths coated with silicalite-1 nanoparticles for benzene adsorption, Microporous Mesoporous Mater. 206 (2015) 184–193.

[53] Z.H. Huang, F. Kang, K.M. Liang, J. Hao, Breakthrough of methyethylketone and benzene vapors in activated carbon fiber beds, J. Hazard. Mater. 98 (2003) 107–115.

[54] Y.H. Yoon, J.H. Nelson, Application of gas adsorption kinetics I. A theoretical model for respirator cartridge service life, Am. Ind. Hyg. Assoc. J. 45 (1984) 509–516.

[55] H.F. Cheng, M. Reinhard, In-line gas chromatographic apparatus for measuring the hydrophobic micropore volume (HMV) and contaminant transformation in mineral micropores, J. Hazard. Mater. 179 (2010) 596–603.

[56] Z.X. Zhao, S. Wang, Y. Yang, X.M. Li, J. Li, Z. Li, Competitive adsorption and selectivity of benzene and water vapor on the microporous metal organic frameworks (HKUST-1), Chem. Eng. J. 259 (2015) 79–89.

[57] K. Kosuge, S. Kubo, N. Kikukawa, M. Takemori, Effect of pore structure in mesoporous silicas on VOC dynamic adsorption/desorption performance, Langmuir 23 (2007) 3095–3102.

[58] B.J. Dou, Q. Hu, J.J. Li, S.Z. Qiao, Z.P. Hao, Adsorption performance of VOCs in ordered mesoporous silicas with different pore structures and surface chemistry, J. Hazard. Mater. 186 (2011) 1615–1624.